

Selective doping Barlowite for quantum spin liquid: a first-principles study

Zheng Liu,^{1,2} Xiaolong Zou,³ Jia-Wei Mei,⁴ and Feng Liu^{2,5}

¹*Institute for Advanced Study, Tsinghua University, Beijing 100084, China*

²*Department of Materials Science and Engineering,
University of Utah, Salt Lake City, UT 84112, USA*

³*Department of Materials Science and Nanoengineering, Rice University, Houston, TX 77005, USA*

⁴*Perimeter Institute for Theoretical Physics, Waterloo, Ontario, N2L 2Y5 Canada*

⁵*Collaborative Innovation Center of Quantum Matter, Beijing 100084, China*
(Dated: September 11, 2018)

Barlowite $\text{Cu}_4(\text{OH})_6\text{FBr}$ is a newly found mineral containing Cu^{2+} kagome planes. Despite similarities in many aspects to Herbertsmithite $\text{Cu}_3\text{Zn}(\text{OH})_6\text{Cl}_2$, the well-known quantum spin liquid (QSL) candidate, intrinsic Barlowite turns out not to be a QSL, possibly due to the presence of Cu^{2+} ions in between kagome planes that induce interkagome magnetic interaction [PRL, 113, 227203 (2014)]. Using first-principles calculation, we systematically study the feasibility of selective substitution of the interkagome Cu ions with isovalent nonmagnetic ions. Unlike previous speculation of using larger dopants, such as Cd^{2+} and Ca^{2+} , we identify the most ideal stoichiometric doping elements to be Mg and Zn in forming $\text{Cu}_3\text{Mg}(\text{OH})_6\text{FBr}$ and $\text{Cu}_3\text{Zn}(\text{OH})_6\text{FBr}$ with the highest site selectivity and smallest lattice distortion. The equilibrium anti-site disorder in Mg/Zn-doped Barlowite is estimated to be one order of magnitude lower than that in Herbertsmithite. The single-electron band structure and orbital component analysis show that the proposed selective doping effectively mitigates the difference between Barlowite and Herbertsmithite.

Quantum spin liquid (QSL) represents a new state of matter characterized by long-range entanglement, beyond the conventional symmetry-breaking paradigm¹. Realizing QSL in real-world materials has been a long-sought goal for decades²⁻⁴. The most promising candidate so far is Herbertsmithite $\text{Cu}_3\text{Zn}(\text{OH})_6\text{Cl}_2$, which realizes the $S = 1/2$ antiferromagnetic (AFM) Heisenberg model on the 2D kagome lattice⁵. Extensive theoretical studies have suggested that this model is likely to achieve a QSL ground-state, despite close in energy with other competing phases⁶⁻¹³. Experiments on Herbertsmithite have also shown QSL-like features, such as the absence of any observed magnetic order down to 50 mK^{14,15} and an unusual continuum of spin excitations¹⁶. However, the inevitable Cu/Zn antisite disorder makes the interpretation of experimental data difficult¹⁷. It remains an open debate whether these defects obscure the intrinsic signals, such as a tiny spin gap that is crucial for the classification of the ground state¹⁸.

Very recently, Barlowite $\text{Cu}_4(\text{OH})_6\text{FBr}$ as a new kagome compound was discovered¹⁹. Its structure closely resembles Herbertsmithite, whereas the Cu/Zn antisite disorder is automatically avoided. Therefore, studies on this new material are expected to shed fresh light on understanding the kagome physics and QSL phase. Interestingly, Barlowite is diagnosed with a Curie-Weiss constant $\theta_{\text{CW}} = -136\text{K}$ close to Herbertsmithite, yet it undergoes a spin-ordering phase transition at 15K²⁰. The low-temperature magnetic properties were further investigated by combining first-principles calculation with experiments²¹. Since the main structural difference between these two materials is the cations occupying the interkagome sites, i.e. Cu^{2+} and Zn^{2+} in Barlowite and Herbertsmithite, respectively, it is suggested that substituting the interkagome sites with nonmagnetic ions

should tune Barlowite into the same phase as Herbertsmithite. Specifically, relatively larger elements, such as Sn and Cd, are speculated as possible candidates for substitution based on the simple argument of lattice spacing of the interkagome sites²⁰.

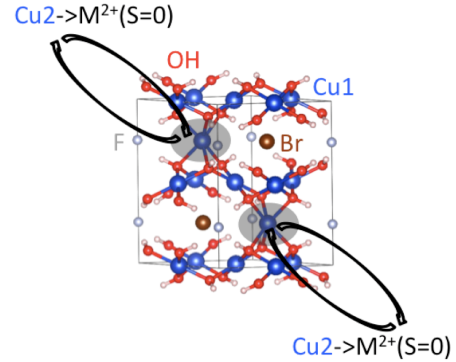


FIG. 1: Unit cell and atomic structure of Barlowite, and the schematic illustration of the proposed selective doping.

In this Letter, we identify the most promising candidates for realizing the selective doping to form stoichiometric doped Barlowite, based on density functional theory (DFT) calculations²². We systematically calculate the doping energies and analyze the doping selectivity of a series of nonmagnetic group 2 and 12 elements. Unlike the previous speculation²⁰, larger dopants are found to have lower site selectivity and tend to distort the kagome plane more than smaller dopants. Most importantly, we identify Mg and Zn to be the most ideal choices of dopants to form stoichiometric $\text{Cu}_3\text{Mg}(\text{OH})_6\text{FBr}$ and $\text{Cu}_3\text{Zn}(\text{OH})_6\text{FBr}$ compounds in the Barlowite family, with the highest site selectivity in substituting the interkagome sites.

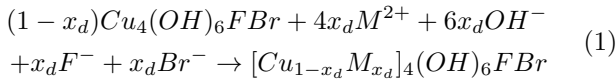
agome Cu ions and the least lattice distortion in kagome planes. Statistical analysis shows that the equilibrium distribution of Mg/Zn in the Mg/Zn-doped Barlowite at the typical growth temperature exhibits a level of antisite disorder significantly lower than that in Herbertsmithite. Also, single-electron band structures of intrinsic and doped Barlowite are calculated, and discussed in comparison with Herbertsmithite.

Figure 1 shows the atomic structure of Barlowite. Similar to Herbertsmithite, it contains Cu^{2+} kagome planes connected by hydroxyls. The difference lies in the interkagome site: in Barlowite, there are additional Cu^{2+} ions between the kagome planes, which act as additional spin 1/2 centers and mediate interkagome spin exchange. Therefore, to clarify the different magnetic ground states between Barlowite and Herbertsmithite, one way is to remove these out-of-plane spins by selective doping. The chosen dopants should be spin zero and isovalent. Using these two criteria, we have considered elements of *Mg*, *Ca*, *Sr*, *Ba* from group 2 and *Zn*, *Cd* from group 12. The ionic radius (r_i) and standard chemical potential in aqueous solution (μ_i^0) of these ions are listed in Tab. I. Note that Mg^{2+} and Zn^{2+} are close in radius to Cu^{2+} , while the other ions are larger. In addition, all these dopants under consideration have a smaller μ_i^0 than Cu^{2+} , indicating a stronger tendency to stay in the solution.

TABLE I: Ionic radius (r_i) and standard chemical potential in aqueous solution (μ_i^0) of Cu and the dopants under consideration

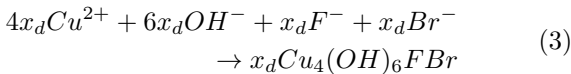
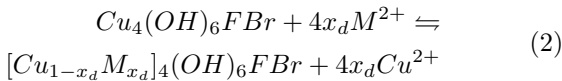
| | r_i (pm) ²³ | μ_i^0 (eV) ²⁴ |
|-----------|--------------------------|------------------------------|
| Cu^{2+} | 73 | 0.68 |
| Mg^{2+} | 72 | -4.73 |
| Ca^{2+} | 100 | -5.73 |
| Sr^{2+} | 118 | -5.78 |
| Ba^{2+} | 135 | -5.81 |
| Zn^{2+} | 74 | -1.52 |
| Cd^{2+} | 95 | -0.80 |

The doping process is expected to take place by adding dopant ions in solution during the hydrothermal growth. The net reaction equation is written as :



in which M^{2+} denotes the dopants.

Equation (1) can be considered as a combination of two subreactions:



Equation (2) describes the simple substitution process. Then, after the Cu ion is exchanged into the solution,

the overall free energy of the system can be lowered by forming more deposits of Barlowite [Eq.(3)]. The latter provides the thermodynamical driving force for the doping process to proceed. Equation (3) is actually nothing but the growth of undoped Barlowite as reported in previous experiments^{20,21}. Hence, we will focus on evaluating the experimental feasibility of Eq.(2) only.

The central physical quantity we are going to calculate is the standard doping energy E_d as defined by the total energy difference per substitution. According to Eq.(2), E_d consists of two parts: $E_d = \Delta E_B + \Delta\mu_i^0$, where $\Delta E_B = (E_{[Cu_{1-x_d}M_{x_d}]_4(OH)_6FBr} - E_{Cu_4(OH)_6FBr})/4x_d$ is the energy change of Barlowite after doping and $\Delta\mu_i^0 = \mu_{Cu^{2+}}^0 - \mu_{M^{2+}}^0$ is the standard chemical potential difference between the two ions (Tab. I). There are two inequivalent doping sites: Cu1 is in the kagome plane; Cu2 is between the kagome planes. We use E_{d1} and E_{d2} to differentiate these two types of doping energies. Their difference $\Delta E_d(x_d) = E_{d1}(x_d) - E_{d2}(x_d)$ tells the site preference for dopants, i.e. defines the degree of selective doping.

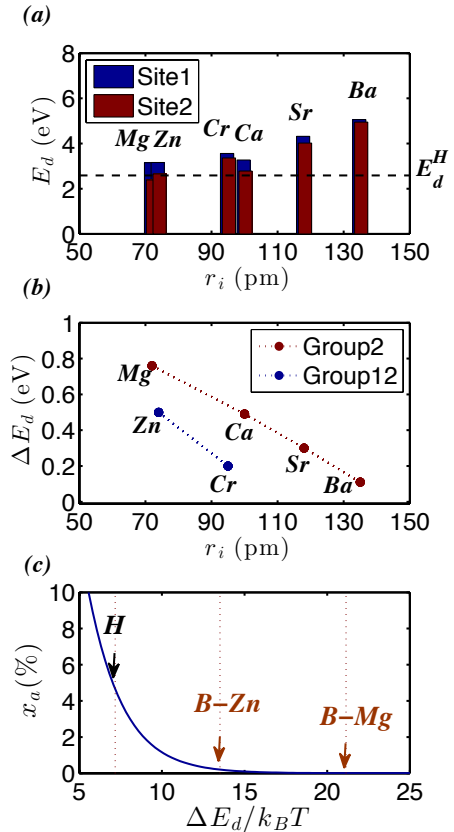


FIG. 2: (a) E_d and (b) ΔE_d of different dopants. E_d^H in (a) corresponds to the standard doping energy for the growth of Herbertsmithite. The dotted line in (b) only serves as a guide to eyes. (c) Equilibrium anti-site disorder of Herbertsmithite (H) and Zn/Mg doped Barlowite (B-Zn/Mg)

Our calculation on ΔE_B is carried out using the VASP package²⁵, which solves the DFT Hamiltonian self-consistently using the plane wave basis together with the projector augmented wave method²⁶. A plane-wave cut-off of 500 eV is enforced. The self-consistent iterations are converged to 0.1 meV precision of the total energy. We employ the standard generalized gradient approximation (GGA) for the exchange-correlation functional, which is known to satisfactorily describe ionic bonding and cohesive energy even for transition elements²⁷. Barlowite stays in the paramagnetic phase above 15K (1meV)^{20,21}. The Dzyaloshinskii-Moriya (DM) interaction arising from spin-orbit coupling is estimated to be of the order of 1 meV²¹. Therefore, a spineless calculation on the structure and total energy is reasonable. As a benchmark, Table 2 summarizes the calculated structural parameters of undoped Barlowite, which agree with the experimental results well. Note that we do not intend to discuss strong correlation effects associated with the Cu 3d orbitals within this methodology.

To simulate doping, we construct a $2 \times 2 \times 1$ supercell containing 24 in-plane Cu1 sites and 8 interkagome Cu2 sites, and replace one of the Cu with a dopant. We first fix lattice constants to experimental values, while let the atomic coordinations fully relax until the forces are less than 0.05 eV/Å. The total-energy integration over the Brillouin zone is obtained on a Γ -centered $2 \times 2 \times 2$ k-mesh.

TABLE II: A comparison of structural parameters between theory and experiment

| Barlowite | Exp. ²⁰ | Exp. ²¹ | Cal. |
|-----------------|--------------------|--------------------|--------|
| Lattice a/b (Å) | 6.68 | 6.80 | 6.73 |
| Lattice c (Å) | 9.31 | 9.31 | 9.47 |
| Angle Cu1-O-Cu1 | 117.4° | 117° | 117.3° |
| Angle Cu1-O-Cu2 | 95.8° | | 96.6° |

Figure 2(a) shows the calculated E_d of different dopants occupying the Cu1 and Cu2 sites. As a reference, we have also calculated the standard doping energy for the growth of Herbertsmithite [E_d^H in Fig. 2(a)] as described by the following equation: $[Cu_{3+x_d}Zn_{1-x_d}](OH)_6Cl_2 + x_d Zn^{2+} \rightleftharpoons Cu_3Zn(OH)_6Cl_2 + x_d Cu^{2+}$. The positive doping energy acts as a reaction barrier, which limits the kinetics of Eq.(1). The value of E_{d2} for Zn is found almost the same as E_d^H , again reflecting the similarities between Barlowite and Herbertsmithite. E_d typically increases with the ionic radius as a size effect: Mg is even easier to substitute Cu than Zn, while larger dopants are more difficult.

The kagome-site doping energy (E_{d1}) is always higher than the interkagome-site doping energy (E_{d2}), indicating that the latter is the preferred site for doping. The preference for dopants to occupy the interkagome site provides exactly the type of doping selectivity we need. It can be understood by noticing the larger space around

the Cu2 site than the Cu1 site (Fig.1). In Fig. 2(b), we plot $\Delta E_d = E_{d1} - E_{d2}$ as a function of ion radius, showing directly the site preference in relation to ionic radius. Within each group, ΔE_d decreases monotonously. The elements from two groups are however not on the same line. This result is reasonable considering that the outermost shells of group 2 and 12 ions are p-electrons and d-electrons, respectively. Thus, they will exhibit different interfacial bonding energy with the surrounding. One important outcome revealed in Fig. 2(d) is that ΔE_d decreases for larger dopants. Therefore, large dopants actually have lower site preference, hence are more difficult to achieve stoichiometric doping. This invalidates the previous speculation²⁰.

One more problem for the large dopants is identified after fully relaxing the lattice volume and geometry. While interkagome doping maintains the original lattice symmetry, the in-plane doping distorts the lattice from hexagonal to triclinic, breaking the perfect kagome plane and lowering the in-plane doping energy. Consequently, ΔE_d becomes smaller. This effect becomes very significant for larger dopants. For example, for Cd^{2+} and Ca^{2+} , ΔE_d decreases from 0.20 and 0.50 eV to -0.12 and 0.11 eV, respectively. It means that upon doping, a large fraction of dopants will substitute the in-plane sites, which in turn distorts the lattice and hinders stoichiometric selective doping. In contrast, for Mg^{2+} and Zn^{2+} , which have similar radius to Cu^{2+} , this problem does not occur: ΔE_d decrease from 0.76 and 0.50 eV to 0.72 and 0.46 eV, respectively, which are still sufficiently large to suppress in-plane doping. Therefore, we conclude that for our purpose Mg^{2+} and Zn^{2+} are the most ideal dopants.

To further examine whether the selective doping of Mg/Zn at the interkagome sites can sustain up to the stoichiometric limit to form $Cu_3Mg(OH)_6FBr$ and $Cu_3Zn(OH)_6FBr$ compounds, we proceed by progressively increasing the amount of interkagome dopants. E_d is found to be nearly independent of the doping concentration (x_d). This property indicates that the interaction between the dopants is weak, which is important for reaching the stoichiometric limit. Otherwise, dopants may form clusters or hinder further doping process. We have also checked that the lattice and Cu kagome planes in $Cu_3Mg(OH)_6FBr$ and $Cu_3Zn(OH)_6FBr$ remain stable under structural relaxation.

It is worth making some comparison to Herbertsmithite within the present methodology. The first critical issue is the degree of equilibrium anti-site disorder in the two systems. The effect of Cu/Zn anti-site disorder in Herbertsmithite has been a long-lasting debate¹⁸. Such disorder is inevitable in doped Barlowite as well, because it leads to an increase of the configuration entropy. Under constant temperature and volume, the equilibrium is reached by minimizing the free energy $F(x_a) = E(x_a) - TS(x_a)$ with respect to the anti-site concentration x_a . Without loss of generality, it is convenient to set $E(0)=S(0)=0$ for the stoichiometric systems. Accordingly, when x_a pairs of Mg(Zn) and Cu per em-

pirical formula switch sites, the energy increase is simply $E(x_a) = x_a \Delta E_d$, given that the interaction between the dopants is weak. The entropy increase per empirical formula can be analytically derived as $S(x_a) = k_B \ln \Omega_a$, where Ω_a is the anti-site configuration number. With the aid of the Sterling's approximation, the final form of entropy is $S(x_a) = -k_B \ln[(3 - x_a)^{3-x_a} (1 - x_a)^{1-x_a} x_a^{2x_a}]$. The minimal point of $F(x_a)$ is calculated numerically, which can be expressed as a function of $\Delta E_d/k_B T$ [Fig. 2(c)]. By using the calculated values of ΔE_d (Mg: 0.72 eV; Zn: 0.46 eV) and the experimental growth temperature ($T=393\text{K}$)²⁰, the anti-site disorder in Mg/Zn doped Barlowite is predicted to be below 0.1%. For comparison, we have also calculated $\Delta E_d = 0.30\text{eV}$ for Herbertsmithite and with $T=483\text{K}$ ⁵, the equilibrium disorder is calculated to be 5%, comparable to the experimental estimation¹⁸. Therefore, the degree of anti-site disorder in the doped Barlowite is expected to be at least one order of magnitude lower than that in Herbertsmithite, owing to a higher ΔE_d as well as a lower growth temperature. This difference can be significant to help clarify the effects of disorder on the QSL phase.

Secondly, we do a comparison of single-electron band structure. Figure 3 shows the band structures of Herbertsmithite, undoped and doped ($x_d = 1$) Barlowite marked with orbital compositions. Despite the absence of strong-correlation effects, the DFT single-electron band structure properly describes single-electron hopping processes, which serve as the guide to the AFM superexchange. For Herbertsmithite, there is a set of bands around the Fermi level (between -0.5 eV and 0.75 eV), gapped from the underlying valence bands²⁸. These bands primarily arise from Cu [blue cross in Fig.3(a)] and the adjacent O (not shown), exhibiting the typical features of NN hopping on a 2D kagome lattice²⁹. For Barlowite [Fig.3(b)], around 0.5 eV the band dispersion is similar to that in Herbertsmithite with the band composition primarily from the

in-plane Cu, indicating similar hopping amplitude within the kagome planes. This is in agreement with the experimental fact that the Curie-Weiss constants for Herbertsmithite and Barlowite are close²⁰. However, around the Fermi level, interkagome Cu not only contributes extra bands, but also strongly mix with the Cu1 bands. This result suggests considerable coupling between Cu1 and Cu2, as pointed out by previous studies^{20,21}. The effect of replacing Cu2 with Zn or Mg is remarkable [Figs.3(c) and (d)]. After doping, the complexities of interkagome coupling are removed. Both Zn and Mg states are far from the Fermi level, leaving clean Cu1 bands around the Fermi level. The overall band dispersion also becomes closer to Herbertsmithite. The energy states below the Fermi level contain contribution from the halogen atoms, i.e. Cl and Br in Herbertsmithite and Barlowite, respectively. We note that both Cl^- and Br^- are spin zero and far away from the superexchange path between Cu1 ions. Therefore, these orbitals do not play an important role in the magnetic properties of the materials.

In conclusion, based on the DFT calculations, we identify $\text{Cu}_3\text{Mg}(\text{OH})_6\text{FBr}$ and $\text{Cu}_3\text{Zn}(\text{OH})_6\text{FBr}$ as the most promising targets to realize the stoichiometric doped Barlowite. The distinct advantages include no lattice distortion, high site selectivity and low anti-site disorder. The standard doping energy is comparable to (for Zn) or even lower (for Mg) than that for growing Herbertsmithite. Therefore, these targets may be readily synthesized using similar experimental conditions as used for Herbertsmithite. The remaining open question is how the doped Barlowite behaves magnetically under low temperature: will it be tuned into the same phase as Herbertsmithite or stay as the undoped Barlowite. For either case, the effective doping of this new material as we propose here serves as a useful guide to future experiments in a pursuit to reveal key factors towards QSL.

-
- ¹ X.-G. Wen, *Quantum Field Theory of Many-body Systems from the Origin of Sound to an Origin of Light and Electrons* (Oxford University Press Inc., New York, 2004), ISBN 019853094.
 - ² P. W. Anderson, *Materials Research Bulletin* **8**, 153 (1973).
 - ³ L. Balents, *Nature* **464**, 199 (2010).
 - ⁴ P. A. Lee, *Science* (New York, NY) **321**, 1306 (2008).
 - ⁵ M. P. Shores, E. A. Nytko, B. M. Bartlett, and D. G. Nocera, *Journal of the American Chemical Society* **127**, 13462 (2005).
 - ⁶ S. Sachdev, *Physical Review B* **45**, 12377 (1992).
 - ⁷ P. Lecheminant, B. Bernu, C. Lhuillier, L. Pierre, and P. Sindzingre, *Physical Review B* **56**, 2521 (1997).
 - ⁸ S. Ryu, O. I. Motrunich, J. Alicea, and M. P. A. Fisher, *Physical Review B* **75**, 184406 (2007).
 - ⁹ Y. Ran, M. Hermele, P. A. Lee, and X.-G. Wen, *Physical Review Letters* **98**, 117205 (2007).
 - ¹⁰ Y.-M. Lu, Y. Ran, and P.-A. Lee, *Physical Review B* **83**, 224413 (2011).
 - ¹¹ S. Yan, D. A. Huse, and S. R. White, *Science* **332**, 1173 (2011).
 - ¹² Y. Iqbal, F. Becca, S. Sorella, and D. Poilblanc, *Physical Review B* **87**, 060405 (2013).
 - ¹³ Y. Iqbal, D. Poilblanc, and F. Becca, *Physical Review B* **89**, 020407 (2014).
 - ¹⁴ J. S. Helton, K. Matan, M. P. Shores, E. A. Nytko, B. M. Bartlett, Y. Yoshida, Y. Takano, A. Suslov, Y. Qiu, J. H. Chung, et al., *Physical Review Letters* **98**, 107204 (2007).
 - ¹⁵ P. Mendels, F. Bert, M. A. de Vries, A. Olariu, A. Harrison, F. Duc, J. C. Trombe, J. S. Lord, A. Amato, and C. Baines, *Physical Review Letters* **98**, 077204 (2007).
 - ¹⁶ T.-H. Han, J. S. Helton, S. Chu, D. G. Nocera, J. A. Rodriguez-Rivera, C. Broholm, and Y. S. Lee, *Nature* **492**, 406 (2012).
 - ¹⁷ A. Olariu, P. Mendels, F. Bert, F. Duc, J. C. Trombe, M. A. de Vries, and A. Harrison, *Physical Review Letters* **100**, 087202 (2008).
 - ¹⁸ P. Mendels and F. Bert, *J. of Phys.: Conference Series*

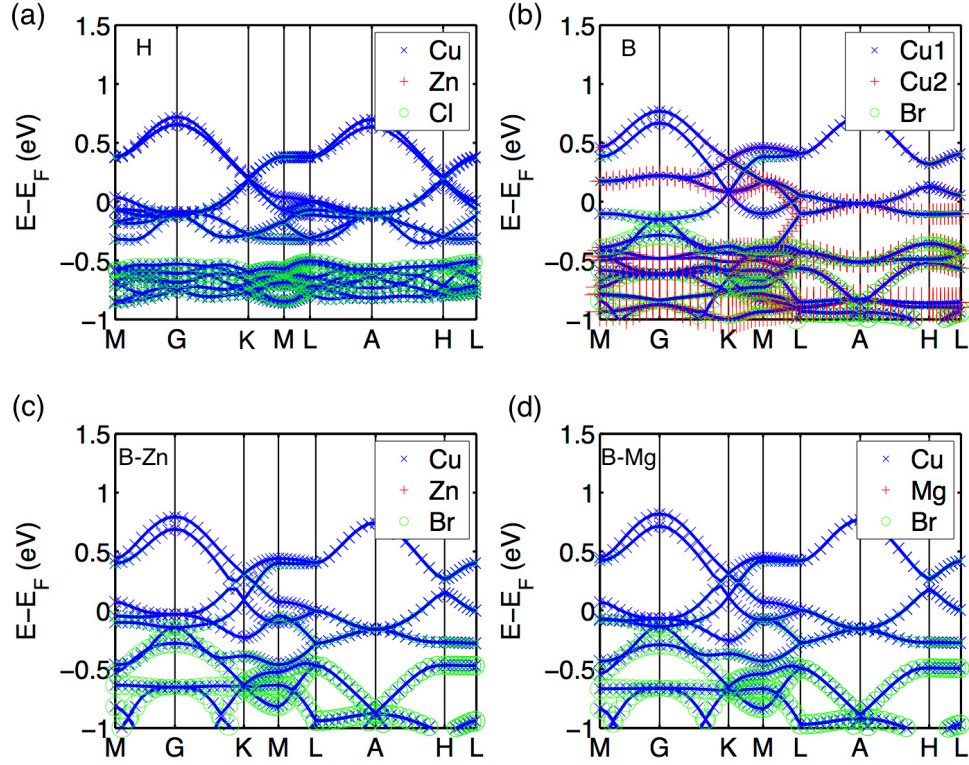


FIG. 3: Orbital resolved single-electron band structure of Herbertsmithite (H), Barlowite (B) and Zn/Mg doped Barlowite (B-Zn/Mg). The marker size reflects the weight of atomic composition.

- 320**, 012004 (2004).
- ¹⁹ P. Elliott, M. A. Cooper, and A. Pring, *Mine. Mag.* **78**, 1755 (2014).
- ²⁰ T.-H. Han, J. Singleton, and J. A. Schlueter, *Physical Review Letters* **113**, 227203 (2014).
- ²¹ J. O. Jeschke, F. Salvat-Pujol, E. Gati, N. H. Hoang, B. Wolf, M. Lang, J. A. Schlueter, and R. Valenti, *arXiv* 1412.4668 (2014).
- ²² R. O. Jones and O. Gunnarsson, *Reviews of Modern Physics* **61**, 689 (1989).
- ²³ R. D. Shannon, *Acta. Cryst.* **A32**, 751 (1976).
- ²⁴ G. Job, *Table of Chemical Potentials*, Eduard-Job Foundation for Thermo and Matter Dynamics, online database: <http://www.job-stiftung.de/index.php?data-collection>.
- ²⁵ G. Kresse and J. Furthmüller, *Physical Review B* **54**, 11169 (1996).
- ²⁶ G. Kresse and D. Joubert, *Physical Review B* **59**, 1758 (1999).
- ²⁷ J. P. Perdew, K. Burke, and M. Ernzerhof, *Physical Review Letters* **77**, 3865 (1996).
- ²⁸ H. O. Jeschke, F. Salvat-Pujol, and R. Valenti, *Physical Review B* **88**, 075106 (2013).
- ²⁹ Z. Liu, F. Liu, and Y.-S. Wu, *Chinese Physics B* **23**, 77308 (2014).